

# Thermodynamics along individual trajectories of a quantum bit

M. Naghiloo,<sup>1</sup> D. Tan,<sup>1</sup> P. M. Harrington,<sup>1</sup> J. J. Alonso,<sup>2</sup> E. Lutz,<sup>2</sup> A. Romito,<sup>3</sup> and K. W. Murch<sup>1,4</sup>

<sup>1</sup>*Department of Physics, Washington University, St. Louis, Missouri 63130*

<sup>2</sup>*Department of Physics, Friedrich-Alexander-Universität Erlangen-Nürnberg, D-91058 Erlangen, Germany*

<sup>3</sup>*Department of Physics, Lancaster University, Lancaster LA1 4YB, United Kingdom*

<sup>4</sup>*Institute for Materials Science and Engineering, St. Louis, Missouri 63130*

(Dated: March 20, 2017)

We use a near-quantum-limited detector to experimentally track individual quantum trajectories of a driven qubit formed by the hybridization of a waveguide cavity and a transmon circuit. For each measured quantum coherent trajectory, we separately identify energy changes of the qubit as heat and work, and verify the first law of thermodynamics for an open quantum system. We further employ a novel quantum feedback loop to compensate for the exchanged heat and effectively isolate the qubit. By verifying the Jarzynski equality for the distribution of applied work, we demonstrate the validity of the second law of thermodynamics. Our results establish thermodynamics along individual quantum trajectories.

The laws of thermodynamics are fundamental laws of nature that classify energy changes for macroscopic systems as work performed by external driving and heat exchanged with the environment. In the past decades, these principles have been successfully extended to the level of classical trajectories of microscopic systems to account for thermal fluctuations [1–3]. In particular, experimentally tested generalizations of the second law [4–6], known as fluctuation theorems, quantify the occurrence of negative entropy production. The extension of thermodynamics to include quantum fluctuations faces unique challenges such as the proper identification of heat and work and clarification of the role of quantum coherence [7, 8]. Here, we present an experimental protocol to measure heat and work along single quantum trajectories of a superconducting qubit evolving under continuous unitary evolution and measurement. We show that the measured heat and work are consistent with the first law and demonstrate the second law in the form of the Jarzynski equality [9] by employing a novel quantum feedback loop. The latter effectively compensates for the heat allowing the work distribution to be inferred from energy measurements. Our results establish thermodynamics along individual quantum trajectories.

In classical thermodynamics, work is defined as the variation of internal energy in an isolated system,  $W = \Delta U$ . For non-isolated systems the first law of thermodynamics introduces heat as the difference,  $Q = \Delta U - W$ . Thermal isolation is thus essential to distinguish heat from work [10]. This definition cannot be directly replicated at the quantum level. Quantum systems do not necessarily occupy definite states and thermodynamic quantities are defined in terms of transition probabilities between energy eigenstates. For a driven quantum system described by the Hamiltonian  $H_t$ , the distribution of the total energy change  $\Delta U$  is [11],

$$P(\Delta U) = \sum_{m,n} P_{m,n}^\tau P_n^0 \delta(\Delta U - (E_m^\tau - E_n^0)), \quad (1)$$

where  $P_n^0$  denote the initial occupation probabilities,  $P_{m,n}^\tau$  are the transition probabilities between initial and final eigenvalues  $E_n^0$  and  $E_m^\tau$  of  $H_t$ , and  $\tau$  is the duration of the protocol. This relation has been used to determine the work distribution and corresponding fluctuation theorems in isolated NMR and trapped ion systems [12, 13] for which  $\Delta U = W$ .

In open quantum systems, the total energy change cannot, in general, be uniquely separated into heat and work [14]. However, for systems whose environment consists of a continuously coupled quantum limited detector, heat and work heat and work may be evaluated along single quantum trajectories [8]. These systems are only weakly coupled to the detector and information about their states  $\tilde{\rho}(t)$  may be inferred the measured signal without projecting them into eigenstates. Such systems might thus generically be in coherent superpositions of energy eigenstates. In this case, the evolution consists of both a unitary part and, because of the continuous monitoring, an additional (nonunitary) stochastic component: the former is identified as work, the latter as heat. Specifically, for an infinitesimal time interval  $dt$ ,  $d\tilde{\rho}_t = \delta\mathbb{W}[\tilde{\rho}_t]dt + \delta\mathbb{Q}[\tilde{\rho}_t]dt$ , where  $\delta\mathbb{W}[\tilde{\rho}_t]$  and  $\delta\mathbb{Q}[\tilde{\rho}_t]$  are superoperators associated with the respective unitary and nonunitary dynamics. The first law along a single quantum trajectory  $\tilde{\rho}(t)$  takes then the form [8],  $d\tilde{U} = \delta\tilde{W} + \delta\tilde{Q}$ , with  $\delta\tilde{W} = \text{tr}[\tilde{\rho}_{t-dt}dH_t]$  and  $\delta\tilde{Q} = \text{tr}[H_t d\tilde{\rho}_t]$  (Methods). When integrated over time, the first law takes the form

$$\Delta U = \int_0^\tau \frac{\delta\tilde{W}}{dt} dt + \int_0^\tau \frac{\delta\tilde{Q}}{dt} dt, \quad (2)$$

for each single quantum trajectory. Equation (2) is a quantum extension of the first law of stochastic thermodynamics. It relates the path-independent change of energy  $\Delta U$  with the path-dependent heat and work. Similarly, we may distinguish heat and work contributions to changes of the transition probabilities,  $d\tilde{P}_{m,n} = \delta\tilde{P}_{m,n}^W + \delta\tilde{P}_{m,n}^Q$ , along individual trajectories (Methods).

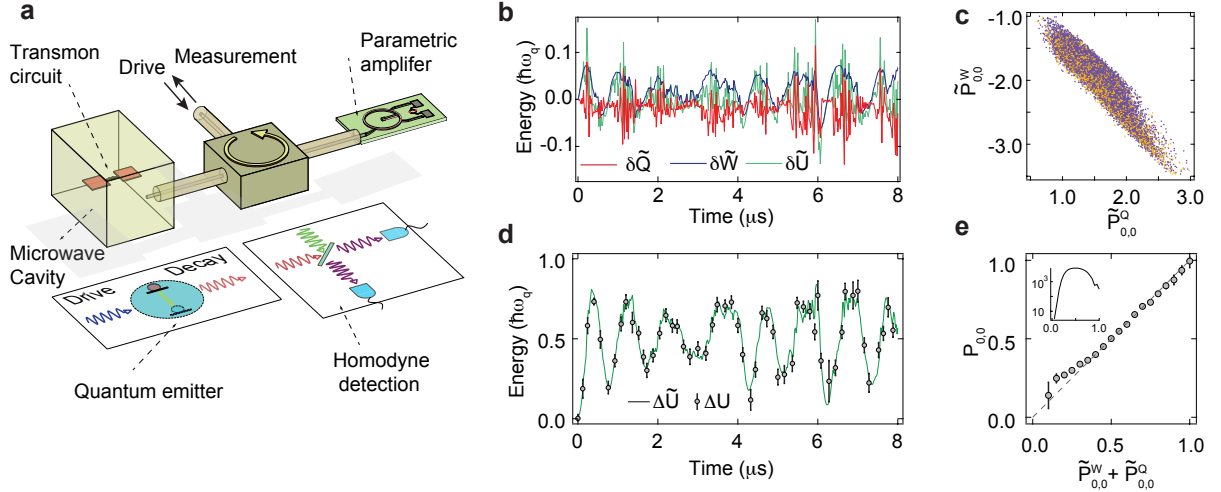


FIG. 1: **Evaluating heat and work along single quantum trajectories.** **a**, Schematic of the qubit system, drive, and homodyne detection. **b**, Instantaneous work (blue), heat (red) and energy (green) along a single trajectory. **c**, A scatter plot of final work and heat contributions to the  $P_{0,0}$  transition probability for an ensemble of  $\sim 10^4$  experimental protocols of duration  $2 \mu\text{s}$ . Each experimental sequence terminates with a projective measurement and the color of the points indicate the outcome of this measurement (orange:  $m = 1$ , purple:  $m = 0$ ). The heat and work contributions are not necessarily bounded, but their sum is limited to  $[-1, 0]$  as expected. **d**, The total energy along a single quantum trajectory (green) compared to the total energy as determined from an ensemble of projective measurements at each time point (circles). The error bars indicate the standard error of the mean. **e**, Projective measurements binned and averaged according to the sum of the work and heat contributions  $\tilde{P}_{0,0}^W + \tilde{P}_{0,0}^Q$ . The agreement with the dashed line demonstrates the first law of thermodynamics. The error bars indicate the standard error of the mean based on the number of occurrences for each value of  $\tilde{P}_{0,0}^W + \tilde{P}_{0,0}^Q$  (inset).

Here we report direct measurements of  $\delta\tilde{W}$  and  $\delta\tilde{Q}$  along individual quantum trajectories of a continuously monitored two-level system. The two-level quantum system is formed by the hybridization of a microwave frequency waveguide cavity and a transmon circuit [15–18], which is described by the Hamiltonian,  $H_q = -\hbar\omega_q\sigma_z/2$ , and depicted in Figure 1(a). The qubit is driven by a classical time-dependent field described by the Hamiltonian  $H_R = \hbar\Omega_R\sigma_y\cos(\omega_q t + \phi)$ , where  $\sigma_z, \sigma_y$  are Pauli matrices,  $\omega_q$  is the resonance frequency of the qubit, and  $\Omega_R$  is the Rabi drive frequency. The qubit is radiatively coupled to a transmission line. Homodyne monitoring of the transmission line using a Josephson parametric amplifier results in weak measurement of the qubit given by the detector signal (Methods),  $dV_t = \sqrt{\eta}\gamma\langle\sigma_x\rangle dt + \sqrt{\gamma}dX_t$ , where  $\eta$  is the quantum efficiency of the homodyne detection,  $\gamma$  is the radiative decay rate, and  $dX_t$  is a zero-mean, Gaussian random variable with variance  $dt$ . The evolution of the qubit, given both driven evolution  $H_R$  and homodyne measurement results  $dV_t$ , is described by the stochastic master equation [19],

$$d\tilde{\rho}_t = -\frac{i}{\hbar}[H_R, \tilde{\rho}_t]dt + \gamma\mathcal{D}[\sigma_-]\tilde{\rho}_t dt + \sqrt{\eta\gamma}\mathcal{H}[\sigma_-dX_t]\tilde{\rho}_t, \quad (3)$$

where  $\mathcal{D}[\sigma_-]\tilde{\rho} = \sigma_-\tilde{\rho}\sigma_+ - \frac{1}{2}(\sigma_+\sigma_-\tilde{\rho} + \tilde{\rho}\sigma_+\sigma_-)$  and  $\mathcal{H}[O]\tilde{\rho} = O\tilde{\rho} + \tilde{\rho}O^\dagger - \text{tr}[(O + O^\dagger)\tilde{\rho}]\tilde{\rho}$  are the dissipation

and jump superoperators, respectively.

Based on the identification of work and heat as the respective unitary and (nonunitary) stochastic contributions to the system evolution, we readily identify the instantaneous work contribution  $\delta W[\tilde{\rho}_t]$  with the first term in (3), while the instantaneous heat contribution  $\delta Q[\tilde{\rho}_t]$  is associated with the latter two terms. Although the system could, in general, exchange energy with the detector in the form of heat or work, the homodyne measurement in our experiment only induces a zero-mean stochastic back-action, which guarantees no extra work is done by the detection process.

Having access to the instantaneous heat and work contributions from a single quantum trajectory, we now verify the first law of thermodynamics in the form of Eq. (2); we perform work by driving the qubit while monitoring the heat exchanged through continuous measurement. For this, we initialize the qubit in the eigenstate  $n$ , and then drive the qubit while collecting the homodyne measurement signal. Figure 1(b) shows the path-dependent instantaneous heat and work contributions,  $\delta\tilde{Q}$  and  $\delta\tilde{W}$ , and the corresponding changes in internal energy  $d\tilde{U}$  for a single quantum trajectory, originating in the state  $n = 0$ . After time  $\tau$  we projectively measure [20] the qubit in state  $m$  and then repeat the experiment several times. In Figure 1(c) we show a scatter plot of the calculated heat and work contributions,  $\tilde{P}_{m,n}^Q$  and  $\tilde{P}_{m,n}^W$

for  $\tau = 2 \mu\text{s}$ . Each trajectory exhibits different heat and work contributions, highlighting the stochastic nature of its quantum evolution.

In Figure 1(d) we show the path-dependent total energy  $\Delta\tilde{U} \equiv \sum \delta\tilde{U}$  for a single trajectory and the path-independent total energy change  $\Delta U \equiv (\hbar\omega_q)P_{1,0}^\tau$  obtained via projective measurements (Methods). We find that the path-independent energy changes are in excellent agreement with the energy changes along a single quantum trajectory. In Figure 1(e) we compare the path-independent transition probabilities to the sum of the path-dependent work and heat contributions for experiments of variable duration  $\tau = [0, 8] \mu\text{s}$ . The close agreement demonstrates the successful identification of heat and work and the verification of the first law.

We next show that the heat and work contributions identified above fulfill the second law of thermodynamics in the form of the Jarzynski equality[9] for a system initially prepared in a thermal state at inverse temperature  $\beta$ ,

$$\langle e^{-\beta W} \rangle = \int P(W) e^{-\beta W} dW = e^{-\beta \Delta F} \quad (4)$$

Equation (4) relates the free energy difference  $\Delta F$  between the equilibrium states of the system defined by  $H_t$  and  $H_0$  to the nonequilibrium work  $W$  done on the system. It is valid arbitrarily far from equilibrium and is an extension of the second law,  $\langle W \rangle \geq \Delta F$ , which follows from (4) via Jensen's inequality [9]. For an open system, the work distribution defined in Eq. (1) does not fulfil the Jarzynski equality due to the heat exchanged with the external environment. The equality (4) may be recovered by compensating the effects of the environment with the help of quantum feedback control [21]. Unit efficiency feedback has been theoretically shown to effectively achieve thermal isolation of the system by suppressing the detector back-action and the resulting heat exchange[8]. At the same time, quantum feedback provides a test of the consistency of the above definitions of heat and work. An incorrect definition of work would indeed lead to a violation of Eq. (4).

The essence of feedback is to adjust the Hamiltonian at each time step to compensate for the effect of the detector,  $\delta Q[\tilde{\rho}_t]$ , thus making the system effectively closed. The dynamics of the system is then simply described by a unitary evolution where only the work  $\delta W[\tilde{\rho}_t]$  contributes. In order to implement feedback, we adapt the phase-locked loop protocol introduced in Ref. [22], schematically depicted in Figure 2(a). This is achieved by multiplying the homodyne measurement signal with a reference oscillator of the form  $A[\sin(\Omega_R t + \phi) + B]$  yielding a feedback control,  $\Omega_F$ , that modulates the amplitude of the qubit drive thereby applying additional work,  $\delta W_F[\tilde{\rho}_t] = (i/\hbar)[\hbar\Omega_F\sigma_y \cos(\omega_q t + \phi), \rho_t]$ , to eliminate exchanged heat.

Figure 2(b) shows the instantaneous feedback work,

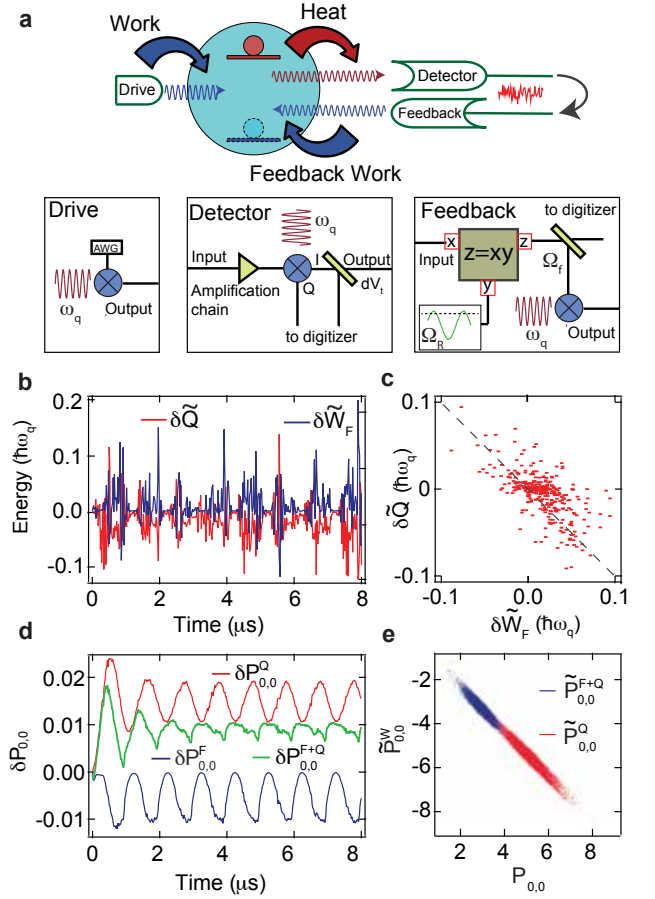


FIG. 2: **Quantum feedback loop.** **a**, Schematic of the feedback protocol. **b**, Instantaneous heat and feedback work along a single trajectory. The feedback work has been time shifted by 20 ns to account for the time delay in the feedback circuit. The anti-correlation ( $r = -0.68$ ) of heat and feedback work is evident in the scatter plot (**c**). **d**, Average of the instantaneous contribution of heat and feedback to the transition probability for  $10^4$  experimental iterations. **e**, Parametric plot of  $\tilde{P}_{0,0}^W$  versus  $\tilde{P}_{0,0}^Q$  (red) and  $\tilde{P}_{0,0}^{F+Q}$  (blue) indicating how the feedback cancels the heat contribution, narrowing and shifting the distribution toward zero for  $\tau = 6 \mu\text{s}$ .

$\delta\tilde{W}_F = \hbar\omega_q \text{tr} [\Pi_{m=1} \delta\mathbb{W}_F[\tilde{\rho}_t]] dt$  (where  $\Pi_m$  is the projector onto eigenstate  $m$ ), together with the corresponding instantaneous heat contribution,  $\delta\tilde{Q} = \hbar\omega_q \text{tr} [\Pi_{m=1} \delta Q[\tilde{\rho}_t]] dt$ , along a single trajectory for a state-of-the-art quantum efficiency of 35%. It is clear from the figure that the feedback partially cancels the heat at each point in time. The anti-correlation between the instantaneous feedback and heat contributions depicted in Figure 2(c) confirms that the feedback loop compensates for exchanged heat at each time step. In addition, by averaging the instantaneous heat and work contributions to the transition probability over many iterations of the experiment (Fig. 2d), we clearly see how feedback works toward canceling the heat contribution

on average.

In the presence of feedback, the work includes both drive and feedback contributions. The total transition probability may be rewritten as  $\tilde{P}_{m,n}^\tau = \tilde{P}_{m,n}^W + \tilde{P}_{m,n}^Q + \tilde{P}_{m,n}^F$ , with the work contribution from feedback  $\tilde{P}_{m,n}^F$ . Figure 2e shows the transition probabilities  $\tilde{P}_{0,0}^W$  versus  $\tilde{P}_{0,0}^Q + \tilde{P}_{0,0}^F$  for about  $10^4$  experiments of duration 6  $\mu\text{s}$ . By comparing the transition probabilities with and without feedback, we observe that the heat contribution is significantly reduced by the feedback. We further note that in the limit of unit quantum efficiency and null loop delay, a feedback loop could exactly compensate for the exchanged heat by the application of additional work, resulting in pure unitary evolution of the qubit (Methods).

We may now use the above feedback protocol to test the Jarzynski equality (4). We first compare the transition probabilities with and without feedback to the expected transition probabilities for a closed system undergoing Rabi oscillations, for which  $P_{11}^t = P_{00}^t = \cos^2(\Omega t)$  and  $P_{10}^t = P_{01}^t = \sin^2(\Omega t)$  (Fig. 3a). We observe that in the absence of feedback (red), the oscillations are damped and the transition probabilities approach the constant value 1/2. On the other hand, in the presence of feedback (blue), the transition probabilities oscillate in agreement with those for the closed system (green), albeit with a smaller amplitude due to finite quantum efficiency.

For our system, the initial and final Hamiltonians are the same and we expect  $\Delta F = 0$ . In Figure 3b we display  $\Delta F$  calculated from the measured transition probabilities with (blue) and without (red) feedback. In the case without feedback,  $\Delta F$  starts from zero, but quickly deviates and then damps into a constant non-zero value  $-0.07\hbar\omega_q$  after a few oscillations, reflecting that the steady state of the driven and dissipated qubit is not purely mixed [23]. In contrast, the feedback strongly suppresses the amplitude of the initial oscillations and reduces the deviation from  $\Delta F = 0$  by a factor of 2 on average. We find from numerical simulations (Methods) that the remaining deviations from the Jarzynski equality are due to the finite efficiency of the feedback protocol and these vanish as the efficiency is improved (Fig. 3b inset).

Our experiment successfully generalizes classical stochastic thermodynamics to the quantum regime. In the confirmation of the first and second laws along individual quantum trajectories, we have allowed for a thermodynamic description of coherent superpositions of energy eigenstates during time evolution, and have demonstrated a practical feedback scheme to consistently distinguish quantum heat from quantum work. Our results pave the way for future experimental and theoretical investigations in information [24] and quantum thermodynamics [25], ranging from the design of microscopic quantum machines [26], the exploration of far from equilibrium quantum phenomena [27] and the interplay of quantum information and energy [28], to the very foun-

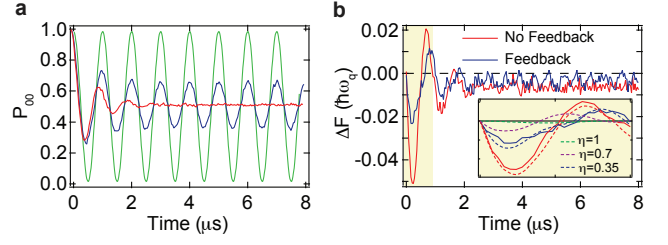


FIG. 3: **Second law of thermodynamics.** **a**, The time evolution of the transition probability  $P_{0,0}$  without feedback (red), with feedback (blue), and ideal unitary evolution (green). **b**, Free energy difference calculated by the Jarzynski equality via the work distribution inferred from the measured transition probabilities at  $\beta/(\hbar\omega_q) = 3.5$ . Feedback reduces the heat contributions to the transition probability showing better agreement with the expected  $\Delta F = 0$ . Simulations (dashed lines, inset) show agreement with the experimental data (solid lines, inset) and indicate how the remaining deviations from the Jarzynski equality vanish as the measurement quantum efficiency is improved.

dations of quantum statistical mechanics and quantum measurement [29].

## METHODS

**Heat and work definitions and contributions to transition probabilities**— The definition of heat and work in the manuscript stems from the association of work with the deterministic driving of the quantum system, and of heat with the stochastic evolution due to the detection process,  $d\tilde{\rho}_t = \delta\mathbb{W}[\tilde{\rho}_t]dt + \delta\mathbb{Q}[\tilde{\rho}_t]dt$ . In fact, the change in the internal energy between times  $t$  and  $t + dt$  along a single quantum trajectory is expressed as

$$\begin{aligned} d\tilde{U}_t &= \text{tr}[H_t(\tilde{\rho}_{t-dt} + d\tilde{\rho}_t)] - \text{tr}[H_{t-dt}\tilde{\rho}_{t-dt}] \\ &= \text{tr}[\tilde{\rho}_{t-dt}dH_t] + \text{tr}[H_t\delta\mathbb{W}dt] + \text{tr}[H_t\delta\mathbb{Q}dt] \\ &= \delta\tilde{W}_t + \delta\tilde{Q}_t, \end{aligned}$$

where in the second line  $dH_t = H_t - H_{t-dt}$  and  $\text{tr}[H_t\delta\mathbb{W}dt] = -\frac{i}{\hbar}\text{tr}[H_t[H_t, \rho_t]dt] = 0$ . In the last line,  $\delta\tilde{W}_t = \text{tr}[\tilde{\rho}_{t-dt}dH_t]$  and  $\delta\tilde{Q}_t = \text{tr}[H_t\delta\tilde{\rho}_t]$ , indicating that work is related to a change of the Hamiltonian, as expected, and heat to the nonunitary changes in the state.

The different contributions of heat and work to the quantum evolution are reflected in different contributions to the transition probabilities. The changes to the transition probabilities due to heat and work are defined as  $\delta\tilde{P}_{m,n}^Q = \text{tr}[\Pi_m\delta\mathbb{Q}[\tilde{\rho}_t]]$ , and  $\delta\tilde{P}_{m,n}^W = \text{tr}[\Pi_m\delta\mathbb{W}[\rho_t]]$ , where  $\Pi_m$  is the projective measurement operator of the eigenstate  $m$  at time  $t$  and the trajectory  $\tilde{\rho}(t)$  originates in eigenstate  $n$ . Correspondingly, we define the path-dependent total transition probabilities,

$$\tilde{P}_{m,n}^Q = \int_0^\tau dt \delta\tilde{P}_{m,n}^Q, \quad \tilde{P}_{m,n}^W = \int_0^\tau dt \delta\tilde{P}_{m,n}^W. \quad (5)$$

The definition of heat and work contributions to the evolution of the density matrix,  $d\tilde{\rho}_t = \delta\mathbb{W}[\tilde{\rho}_t]dt + \delta\mathbb{Q}[\tilde{\rho}_t]dt$ , imply that, starting from a density matrix  $\rho_0$  corresponding to an eigenstate  $n$ , the total transition probabilities  $\tilde{P}_{m,n}^\tau$  are expressed as

$$\begin{aligned}\tilde{P}_{m,n}^\tau &= \text{tr}[\Pi_m \tilde{\rho}_t] = P_{m,n}^0 + \int_0^\tau dt \text{tr}[\Pi_m \delta\mathbb{Q}[\tilde{\rho}_t]]dt \\ &+ \int_0^\tau dt \text{tr}[\Pi_m \delta\mathbb{W}[\tilde{\rho}_t]]dt = \tilde{P}_{m,n}^Q + \tilde{P}_{m,n}^W,\end{aligned}$$

The instantaneous heat, work, and feedback are also expressed in terms of energy by  $\delta\tilde{Q} = \hbar\omega_q \text{tr}[\Pi_{m=1} \delta\mathbb{Q}[\tilde{\rho}_t]]$ ,  $\delta\tilde{W} = \hbar\omega_q \text{tr}[\Pi_{m=1} \delta\mathbb{W}[\tilde{\rho}_t]]$ , and  $\delta\tilde{W}_F = \hbar\omega_q \text{tr}[\Pi_{m=1} \delta\mathbb{W}_F[\tilde{\rho}_t]]$ , respectively. These changes reflect only the instantaneous changes in energy and do not depend on the initial state of the system.

Transmission probabilities can be experimentally obtained by preparing the qubit in a specific initial state  $n$  and terminating the experiment at time  $\tau$  with a projective measurement [20] in the energy basis. These projective measurements allow us to determine the total energy difference for the qubit and compare to the total energy calculated from the heat and work along individual quantum trajectories, in a manner similar to the tomographic validation for trajectories in previous work [30, 31]. In Figure 1d we show the total energy changes of the qubit  $\Delta U$  obtained from the transition probability  $P_{1,0}$  which was determined from an ensemble of  $10^5$  experiments of variable duration  $\tau$  where the path-dependent energy  $\tilde{U}$  was within  $\pm 0.05$  of the black curve shown in Figure 1d at time  $\tau$ . The transition probability is corrected for the finite readout fidelity of 65%. In Figure 1e, we compare the measured, path-independent, transition probability  $P_{0,0}$ , to the path-dependent transition probability  $\tilde{P}_{0,0}^W + \tilde{P}_{0,0}^Q$ , by binning experiments of variable duration according to the final path-dependent transition probability and determining the transition probability  $P_{0,0}$  at each point from the outcomes of the projective readout. The close agreement between  $P_{0,0}$  and  $\tilde{P}_{0,0}^W + \tilde{P}_{0,0}^Q$  indicates that the two independent measures of the qubit energy are in agreement, thereby confirming the first law of thermodynamics.

**Homodyne detection**—The qubit is realized by the near-resonant interaction of a transmon circuit [15] and a three-dimensional aluminum cavity [16] which is coupled to a  $50\ \Omega$  transmission line. The radiative interaction between the qubit and transmission line is given by the interaction Hamiltonian,  $H_{\text{int.}} = \hbar\gamma(a\sigma_+ + a^\dagger\sigma_-)$ , where  $\gamma$  is the coupling rate between the electromagnetic field mode corresponding to  $a$  ( $a^\dagger$ ), the annihilation (creation) operator, and qubit state transitions by  $\sigma_+$  ( $\sigma_-$ ), the raising (lowering) ladder operator for the qubit. By virtue of this interaction Hamiltonian, a homodyne measurement along an arbitrary quadrature of the quantized electromagnetic field of the transmission line,

$ae^{-\phi} + a^\dagger e^{+\phi}$ , results in weak measurement along the corresponding dipole of the qubit,  $\sigma_+ e^{-\phi} + \sigma_- e^{+\phi}$  [18]. Homodyne monitoring is performed with a Josephson parametric amplifier [32, 33] operated in phase-sensitive mode. We adjust the homodyne detection quadrature such that the homodyne signal  $dV_t$  obtained over the time interval  $(t, t + dt)$  provides an indirect signature [34] of the real part of  $\sigma_- = (\sigma_x + i\sigma_y)/2$ . The detector signal is given by  $dV_t = \sqrt{\eta}\gamma\langle\sigma_x\rangle dt + \sqrt{\gamma}dX_t$ , where  $dX_t$  is a zero-mean Gaussian random variable that arises due to the quantum fluctuations of the field mode.

**Heat and work tracking**—The stochastic master equation (Eq. 3) is used to update state of the qubit conditioned on the collected homodyne signal which is digitized in 20 ns steps, and scaled such that its variance is  $\gamma dt$ . Our identification of work and heat as the respective unitary and stochastic changes of the state applies in the laboratory frame. However, it is convenient to calculate the state trajectories in the frame rotating with the qubit drive, yet we can still identify these energy changes in the rotating frame. The discretized stochastic master equation (in Itô form) is used to obtain evolution of the qubit in the rotating frame [35].

$$\begin{aligned}d\tilde{\rho}_{00}[i] &= \Omega\tilde{\rho}_{01}[i]dt + \gamma(1 - \tilde{\rho}_{00}[i])dt \\ &+ \sqrt{\eta}(dV[i] - \sqrt{\eta}\gamma 2\tilde{\rho}_{01}[i]dt) \\ &\times 2\tilde{\rho}_{01}[i](1 - \tilde{\rho}_{00}[i]),\end{aligned}\tag{6}$$

$$\begin{aligned}d\tilde{\rho}_{01}[i] &= \Omega(1/2 - \tilde{\rho}_{00}[i])dt - \gamma\tilde{\rho}_{01}[i]/2dt \\ &+ \sqrt{\eta}(dV[i] - \sqrt{\eta}\gamma 2\tilde{\rho}_{01}[i]dt) \\ &\times (1 - \tilde{\rho}_{00}[i] - 2\tilde{\rho}_{01}^2[i]).\end{aligned}\tag{7}$$

Each time-step  $i$  is divided into two sub-steps. The first sub-step updates the  $\tilde{\rho}(t)$  by the unitary terms. Subsequently, in the second sub-step  $\tilde{\rho}(t)$  is updated by the nonunitary terms [8]. Therefore, in each time step, we accordingly distinguish between instantaneous work and instantaneous heat and can determine these energy changes in the lab frame.

**Feedback**—In this section, we analyse in detail the feedback protocol used in the experiment and compare it with optimal feedback protocols in the presence of finite efficiency and feedback loop delay.

If  $\eta = 1$  the state of the system is pure at any time, and is described by a vector on the surface of the Bloch sphere. An ideal feedback loop would then exactly and immediately compensate for the heat exchanged with the environment resulting in completely unitary evolution of the state. This is not possible at finite inefficiency, where the evolution of the system is no longer constrained to the surface of the Bloch sphere. Since the evolution due to the feedback protocol is unitary, it preserves the length of the Bloch vector, and cannot restore unitary evolution once purity has been lost. Therefore, it is impossible to exactly compensate for the exchanged heat with a unitary



operation.

Given access to the trajectory in real time, the best possible feedback is to maintain the phase of the oscillation as if it were to undergo closed unitary evolution (Fig. 4a). In this case, the feedback output would be  $\Omega_F dt = -\theta_Q$  where  $\theta_Q$  can be calculated by the state of the qubit at  $t$  and  $t + dt$ . In this case we would not have control over the purity of the state and it will change by measurement back-action from point to point. Figure 4 shows simulation results for this type of feedback for 35% quantum efficiency. As depicted in Figure 4b, the exchanged heat contribution is compensated by the feedback contribution. The scatter plot in Figure 4(c) shows the anti-correlation of these contributions. Therefore, as we expect, the system will behave more like a closed system and we observe persistent Rabi oscillations with 70% of full contrast (Fig. 4d). However, a realistic feedback loop would also have a finite loop delay, given by the time it takes for the measurement signal to travel to a detector and for the feedback output to be calculated. Considering a feedback loop delay of  $\sim 500$  ns [36, 37], Figure 4(d) (blue curve) shows that the feedback performance would be reduced.

The feedback loop implemented in our experiment differs from the optimal feedback in that it does not require real-time state tracking and error processing. This feedback takes a copy of homodyne signal,  $dV_t$ , and multiplies it by a sinusoidal reference signal,  $A[\sin(\Omega_R t + \phi) + B]$  resulting in a feedback signal  $\Omega_F$ , which is used to modulate the drive amplitude.

This feedback loop essentially implements a phase-locked loop, and in order to clarify how the loop works we may cast the stochastic master equation (3) in terms of the Bloch components  $x$  and  $z$ ,

$$\begin{aligned} dz &= +\Omega x dt \\ &+ \gamma(1-z)dt + \sqrt{\eta}x(1-z)(dV_t - \gamma\sqrt{\eta}xdt) \\ dx &= -\Omega z dt \\ &- \frac{\gamma}{2}xdt + \sqrt{\eta}(1-z-x^2)(dV_t - \gamma\sqrt{\eta}xdt). \end{aligned} \quad (8)$$

It is apparent that by canceling the last two terms, the evolution would be a completely unitary evolution as we expect from a closed system. However, with only unitary rotations we can change  $dz$  and  $dx$  in the following way,

$$dz = \Omega_F x dt, \quad dx = -\Omega_F z dt, \quad (9)$$

where, we wish to cancel all the stochastic terms in (8) with the unitary terms (9). Regardless how complicated  $\Omega_F$  is, with finite efficiency, it is impossible to compensate for all terms as mentioned earlier and the best choice recovers about 70% of contrast for 35% quantum efficiency. To understand how the phase-locked loop approximates the optimal feedback, we consider just the  $z$  component of the state. This is reasonable since all thermodynamics parameters e.g. work, heat and transition

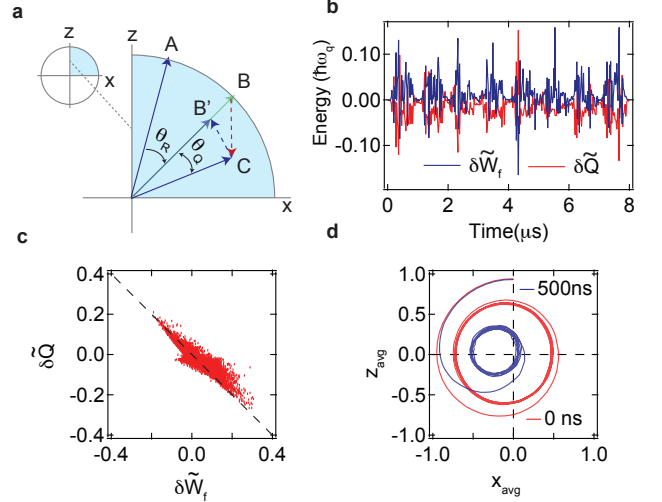


**FIG. 4: Simulation of optimal unitary feedback.** **a**, Schematic of the feedback operation, the qubit evolution from  $A$  at time  $t$  to  $C$  at time  $t + dt$  comprises of two different type of evolution; a unitary evolution due to the Rabi drive ( $A \rightarrow B$ ) and a stochastic evolution due to coupling to the environment. Because the environment is monitored with sub-unity quantum efficiency we effectively average over some of the stochastic evolution reducing the state purity ( $B \rightarrow C$ ). The ideal unitary feedback maintains the phase relation with unitary evolution by application of a rotation  $-\theta_Q$  to state  $B'$ . **b**, Instantaneous contribution of heat and feedback to the transition probability  $P_{0,0}$  for a single run of experiment. **c**, Scatter plot of the instantaneous heat versus feedback for 100 runs of experiment which shows anti-correlation ( $r = -0.9$ ) between feedback and heat contribution to transition probability  $P_{00}$ . **d**, Ensemble behavior of the trajectories in presence of feedback with no delay (red) and 500 ns loop delay (blue) showing a persistent Rabi oscillations.

probabilities directly relate to the  $z$  component. This requires  $\Omega_F x dt = -\sqrt{\eta}x(1-z)(dV_t - \gamma\sqrt{\eta}xdt)$ , where for weak measurement  $\gamma\sqrt{\eta}xdt$  is negligible compared to  $dV_t$ . Thus, we have  $\Omega_F = -\sqrt{\eta}(1-z)dV_t/dt$ . The essence of the phase-locked loop is to replace  $z$  with  $\cos(\Omega t + \phi)$ , which is the “target”  $z$  that would be obtained for closed evolution. Here  $\phi = 0$  ( $\pi$ ) for an initial ground (excited) state. This choice for  $z$  has two-fold effect: not only it is a reasonable approximation for  $z$  in presence of feedback but it also locks the phase of oscillation which addresses the damping term in (8). Note that the choice of phase  $\phi$  only affects the transient behavior and appears as a overall phase shift in the persistent Rabi oscillations without affecting the contrast. Thus the feedback signal is,

$$\Omega_F = \sqrt{\eta}(\cos(\Omega t + \phi) - 1)dV_t/dt, \quad (10a)$$

This equation suggests that the scale for feedback should be around  $A = \sqrt{\eta}/dt \sim 30$  which is in agreement with optimal value found empirically in the experiment of  $A = 34$ . Experimentally, this factor may be set by pre-amplification of homodyne signal. Note that this result

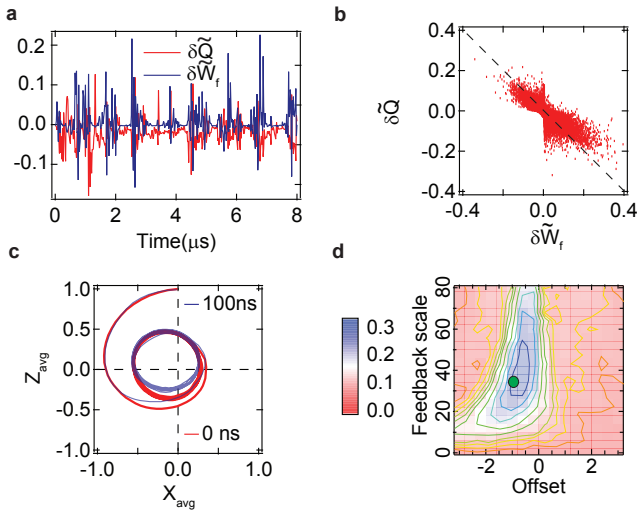


FIG. 5: **Simulation of phase-lock feedback.** **a**, Instantaneous contribution of heat and feedback to the transition probability  $P_{0,0}$  for a single run of experiment. **b**, Scatter plot of instantaneous heat versus feedback for 100 runs of experiment which shows anti-correlation ( $r = -0.81$ ) between the feedback and heat contributions to transition probability  $P_{0,0}$ . **c**, Ensemble behavior of the trajectories in presence of feedback with no delay (red) and 100 ns loop delay (blue) showing a persistent Rabi oscillations. **d**, Simulated feedback efficiency versus feedback scale ( $A$ ) and offset ( $B$ ). The green dot indicates the expected parameters for optimal feedback.

also suggests the offset term of  $B = -1$  as we use in our feedback setup. Figure 5 shows the simulation result for the phase-locked feedback with 35% quantum efficiency.

As we see in Figure 5(a,b), the phase-locked feedback loop effectively compensates for the heat at each point in time. Figure 5(c) shows persistent Rabi oscillations for this case. In Figure 5(d), we explore the contrast of persistent Rabi oscillations versus feedback parameters: feedback scale and offset. The simulated result shows that maximum contrast occurs around  $B \sim -1$  and  $A \sim 35$  as we expect.

**Jarzynski equality at higher quantum efficiency**—In Figure 3 we show the change in free energy obtained for different values of the quantum efficiency. We find that the remaining violations of the Jarzynski equality are reduced as the quantum efficiency is increased. For the simulations with non-unity quantum efficiency, we use the Itô form of stochastic master equation (Eqs. 8) to simulate trajectories for finite efficiencies, which is consistent with the state update used in the experiment. For the unity efficiency feedback simulation we instead use the Stratonovich form of the stochastic master equation [34].

**Experimental setup and parameters**—The transmon circuit was fabricated using double angle evaporation of aluminum on a high resistivity silicon substrate. The circuit was placed at the center of a 3D aluminum

waveguide cavity which was machined from 6061 aluminum. The bare cavity frequency is  $\omega_c/2\pi = 7.257$  GHz. The near-resonant interaction between the circuit and the cavity (characterized by coupling rate  $g/2\pi = 136$  MHz) results in hybrid states, as described by the Jaynes-Cummings Hamiltonian. The lowest energy transition of hybrid states ( $\omega_q/2\pi = 6.541$  GHz) can therefore be considered a “one-dimensional” artificial atom because the radiative decay of the system is dominated by the cavity’s coupling to a  $50 \Omega$  transmission line, characterized by a quality factor  $Q = 630$ . This radiative decay was characterized by a decay of rate  $\gamma = 1.7 \mu s^{-1}$ . Resonance fluorescence from the artificial atom is amplified by a near-quantum-limited Josephson parametric amplifier, consisting of a  $1.5$  pF capacitor, shunted by a Superconducting Quantum Interference Device (SQUID) composed of two  $I_0 = 1 \mu A$  Josephson junctions. The amplifier produces 20 dB of gain with an instantaneous 3-dB-bandwidth of 50 MHz. The quantum efficiency was measured to be 35%. We drive the qubit by sending a resonant coherent signal via a weakly coupled transmission line, and the strength of the drive is characterized by a Rabi frequency of  $\Omega/2\pi \simeq 1$  MHz. The total loop delay for the feedback is 100 ns. The initial state fidelity was limited by a 3% thermal population of the excited state.

**Acknowledgements:** We acknowledge research support from the NSF (grant PHY-1607156) the ONR (grant No. 12114811), the John Templeton Foundation, the EU Collaborative Project TherMiQ (Grant Agreement 618074) and the COST Action MP1209. This research used facilities at the Institute of Materials Science and Engineering at Washington University. K.M. acknowledges support from the Sloan Foundation.

Correspondence and requests for materials should be addressed to [murch@physics.wustl.edu](mailto:murch@physics.wustl.edu).

- 
- [1] Jarzynski, C. Equalities and inequalities: Irreversibility and the second law of thermodynamics at the nanoscale. *C. Annu. Rev. Condens. Matter Phys.* **2**, 329 (2011).
  - [2] Seifert, U. Thermodynamics, fluctuation theorems and molecular machines. *Rep. Prog. Phys.* **75**, 126001 (2012).
  - [3] Ciliberto, S., Gomez-Solano, R. & Petrosyan, A. Fluctuations, linear response, and currents in out-of-equilibrium systems. *C. Annu. Rev. Condens. Matter Phys.* **4**, 235 (2013).
  - [4] Liphardt, J., Dumont, S., Smith, S. B., Tinoco, I. & Bustamante, C. Equilibrium information from nonequilibrium measurements in an experimental test of Jarzynski’s equality. *Science* **296**, 1832–1835 (2002).
  - [5] Wang, G. M., Seifert, E. M., Mittag, E., Searles, D. J. & Evans, D. J. Experimental demonstration of violations of the second law of thermodynamics for small systems and short time scales. *Phys. Rev. Lett.* **89**, 050601 (2002).
  - [6] Blickle, V., Speck, T., Helden, L., Seifert, U. &

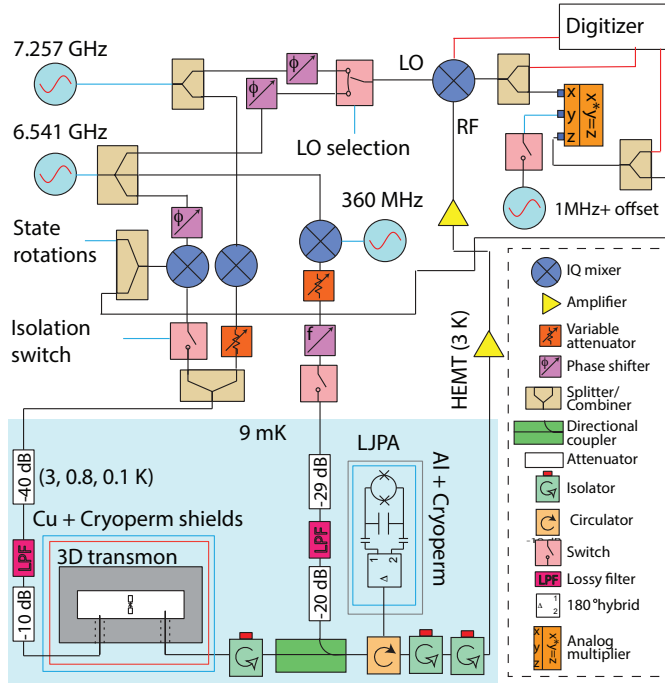


FIG. 6: **Experimental setup** The qubit and Josephson parametric amplifier share a signal generator to maintain the phase relation defining the amplification quadrature. We use a double side-band technique to pump the parametric amplifier. The homodyne signal is split in two for the purpose of feedback and state tracking. Both the feedback signal and homodyne signal are digitized for state tracking in a post-processing step.

- Bechinger, C. Thermodynamics of a colloidal particle in a time-dependent nonharmonic potential. *Phys. Rev. Lett.* **96**, 070603 (2006).
- [7] Gallego, R., Eisert, J. & Wilming, H. Thermodynamic work from operational principles. *New Journal of Physics* **18**, 103017 (2016).
- [8] Alonso, J. J., Lutz, E. & Romito, A. Thermodynamics of weakly measured quantum systems. *Phys. Rev. Lett.* **116**, 080403 (2016).
- [9] Jarzynski, C. Nonequilibrium equality for free energy differences. *Phys. Rev. Lett.* **78**, 2690–2693 (1997).
- [10] Pippard, A. B. *Elements of Classical Thermodynamics* (Cambridge, 1966).
- [11] Talkner, P., Lutz, E. & Hänggi, P. Fluctuation theorems: Work is not an observable. *Phys. Rev. E* **75**, 050102 (2007).
- [12] Batalhão, T. B. *et al.* Experimental reconstruction of work distribution and study of fluctuation relations in a closed quantum system. *Phys. Rev. Lett.* **113**, 140601 (2014).
- [13] An, S. *et al.* Experimental test of the quantum Jarzynski equality with a trapped-ion system. *Nature Physics* **11**, 193199 (2015).
- [14] Campisi, M., Hänggi, P. & Talkner, P. Quantum fluctuation relations: Foundations and applications. *Rev. Mod. Phys.* **83**, 771–791 (2011).
- [15] Koch, J. *et al.* Charge-insensitive qubit design derived from the Cooper pair box. *Phys. Rev. A* **76**, 042319 (2007).
- [16] Paik, H. *et al.* Observation of high coherence in Josephson junction qubits measured in a three-dimensional circuit QED architecture. *Phys. Rev. Lett.* **107**, 240501 (2011).
- [17] Murch, K. W., Weber, S. J., Beck, K. M., Ginossar, E. & Siddiqi, I. Reduction of the radiative decay of atomic coherence in squeezed vacuum. *Nature* **499**, 62–65 (2013).
- [18] Naghiloo, M., Foroozani, N., Tan, D., Jadbabaie, A. & Murch, K. W. Mapping quantum state dynamics in spontaneous emission. *Nature Communications* **7**, 11527 (2016).
- [19] Bolund, A. & Mølmer, K. Stochastic excitation during the decay of a two-level emitter subject to homodyne and heterodyne detection. *Phys. Rev. A* **89**, 023827 (2014).
- [20] Reed, M. D. *et al.* High-fidelity readout in circuit quantum electrodynamics using the Jaynes-Cummings nonlinearity. *Phys. Rev. Lett.* **105**, 173601 (2010).
- [21] H. W. Wiseman, G. M. *Quantum Measurement and Control* (Cambridge, 2010).
- [22] Vijay, R. *et al.* Stabilizing Rabi oscillations in a superconducting qubit using quantum feedback. *Nature* **490**, 77 (2012).
- [23] Gardiner, C. W. Inhibition of atomic phase decays by squeezed light: A direct effect of squeezing. *Phys. Rev. Lett.* **56**, 1917–1920 (1986).
- [24] Parrondo, J. M. R., Horowitz, J. M. & Sagawa, T. Thermodynamics of information. *Nature Physics* **11**, 131 (2015).
- [25] J. Gemmer, G. M., M. Michel. *Quantum Thermodynamics* (Springer, 2004).
- [26] Kosloff, R. & Levy, A. Quantum heat engines and refrigerators: Continuous devices. *Annual Review of Physical Chemistry* **65**, 365–393 (2014).
- [27] Esposito, M., Harbola, U. & Mukamel, S. Nonequilibrium fluctuations, fluctuation theorems, and counting statistics in quantum systems. *Rev. Mod. Phys.* **81**, 1665–1702 (2009).
- [28] Goold, J., Huber, M., Riera, A., del Rio, L. & Skrzypczyk, P. The role of quantum information in thermodynamics - a topical review. *Journal of Physics A: Mathematical and Theoretical* **49**, 143001 (2016).
- [29] Dressel, J., Chantasri, A., Jordan, A. N. & Korotkov, A. N. Arrow of time for continuous quantum measurement arXiv:1610.03818 (2016).
- [30] Murch, K. W., Weber, S. J., Macklin, C. & Siddiqi, I. Observing single quantum trajectories of a superconducting qubit. *Nature* **502**, 211 (2013).
- [31] Weber, S. J. *et al.* Mapping the optimal route between two quantum states. *Nature* **511**, 570–573 (2014).
- [32] Castellanos-Beltran, M. A., Irwin, K. D., Hilton, G. C., Vale, L. R. & Lehnert, K. W. Amplification and squeezing of quantum noise with a tunable Josephson metamaterial. *Nature Physics* **4**, 929–931 (2008).
- [33] Hatridge, M., Vijay, R., Slichter, D. H., Clarke, J. & Siddiqi, I. Dispersive magnetometry with a quantum limited squid parametric amplifier. *Phys. Rev. B* **83**, 134501 (2011).
- [34] Jordan, A. N., Chantasri, A., Rouchon, P. & Huard, B. Anatomy of fluorescence: quantum trajectory statistics from continuously measuring spontaneous emission. *Quantum Studies: Mathematics and Foundations* 1–27



- (2015).
- [35] Naghiloo, M. *et al.* Quantum caustics in resonance fluorescence trajectories. *arXiv:1612.03189* (2016).
- [36] Campagne-Ibarcq, P. *et al.* Persistent control of a superconducting qubit by stroboscopic measurement feedback. *Phys. Rev. X* **3**, 021008 (2013).
- [37] Ristè, D., Bultink, C. C., Lehnert, K. W. & DiCarlo, L. Feedback control of a solid-state qubit using high-fidelity projective measurement. *Phys. Rev. Lett.* **109**, 240502 (2012).